INSTITUTE OF PHYSICS PUBLISHING PHYSICS IN MEDICINE AND BIOLOGY

Phys. Med. Biol. **48** (2003) 1997–2011 PII: S0031-9155(03)61547-2

High-resolution EEG mapping: an equivalent charge-layer approach

Dezhong Yao

School of Life Science and Technology, University of Electronic Science and Technology of China, Chengdu 610054, People's Republic of China

E-mail: dyao@uestc.edu.cn

Received 1 April 2003
Published 17 June 2003
Online at stacks.iop.org/PMB/48/1997

Abstract

Brain electrical signal is one of the windows to understanding neural activities. Various high-resolution imaging techniques have been developed to reveal the electrical activities underneath the cortical surface from scalp electroencephalographic recordings, such as scalp Laplacian, cortical surface potential, equivalent charge layer (ECL) and equivalent dipole layer (EDL). In this work, we develop forward density formulae for the ECL and the EDL of neural electric sources in a 4-concentric-sphere head model, and compare ECL with EDL in theory, simulation and real evoked data tests. The results confirm that the ECL map may be of higher spatial resolution than the EDL map.

1. Introduction

Electroencephalography (EEG) and evoked potential (EP) are important tools for diagnosing or exploring the function of the nervous system regarding normal or pathological conditions (Niedermeyer and Lopes da Silva 1999). The spatial or topographical features provide access to the detection of focal EEG phenomena that have a relationship to focal pathology (Niedermeyer and Lopes da Silva 1999) or localized brain function (Nunez 1989, Yao 2000). A number of interpolation methods have been developed for constructing the scalp EEG and EP maps from the scalp potential recordings. The quality and spatial resolution of such a potential map are therefore largely dependent on the interpolation technique and the number of recording channels. While, due to spatial smearing and other distortions existing in the head volume conductor (Yao 2000), additional recording electrodes may not necessarily lead to an improvement of the spatial resolution (Nunez *et al* 1994), therefore further steps are needed to get a higher spatial resolution map.

A few approaches have been developed to construct a noninvasive high-resolution imaging map, which have been increasingly used in recent years. One popular imaging modality is *scalp Laplacian mapping* (*LM*), which is based on the 2D Laplace operation on the scalp

potential, thus offering a higher spatial resolution map than that with the conventional scalp EEG map (Hjorth 1975). LM is theoretically related to the scalp current density by a function of spatial frequency, and for practically available low spatial frequencies, they are approximately linearly related to each other (Yao 2002a, 2002b).

Another important kind of mapping technique is high-resolution potential mapping, including source potential mapping (SPM) (Yao 2001), which images the neural sources by the potential produced by the actual sources in a homogeneous infinite conducting medium, and cortical potential mapping (CPM), which images the sources by the cortical surface potential produced by the actual sources in the real head model (Sidman *et al* 1992). Various approaches have been developed to reconstruct SPM or CPM from the scalp recordings, such as the equivalent dipole-layer (EDL) technique (Sidman *et al* 1992), and the equivalent charge-layer (ECL) technique (Yao 1996).

The third kind of mapping technique is equivalent layer source imaging, i.e., EDL and ECL, especially EDL. They have been tested not only as an intermediate step to get SPM and CPM, but also as an imaging quantity directly (Hamalainen and Ilmoniemi 1984, Nunez 1987, Wang *et al* 1992, Dale and Sereno 1993, Babiloni *et al* 2000, Yao *et al* 2001, He *et al* 2002a).

In this paper, our focus is the ECL approach for high-resolution electroencephalographic mapping, and the physiological explanation of the charge source model used in ECL may be a concern. As the brain or body is a volume conductor, there is no static charge or dipole, but current in the tissues. For an active neuron in a conductive tissue, the total current $\vec{J}$ consists of two parts (Plonsey 1969): a primary (or driving) current flow $\vec{J}^p$ related to the original neural activity and a volume (or passive) current flow $\vec{J}^V$ that results from the effect of the electric field in the volume on extracellular charge carriers ($\vec{J} = \vec{J}^V + \vec{J}^p$). The primary current flows in the neuron and the volume current (secondary current) flows in the volume conductor (tissues). The two currents ($\vec{J}^p$ and $\vec{J}^V$) work together forming a closed current loop that makes the divergence of the total current $\vec{J}$ vanish $\nabla \cdot \vec{J} = 0$ (Plonsey 1969), so there is no charge accumulation in a biological tissue, which makes the net charge in any volume zero.

In general, the current is time varying, the basic theory of brain electricity should be the Maxwell equations. However, because the change of the neural current is slow, a 'quasi-static' approximation is commonly used in EEG and MEG practice (Plonsey 1969). For a stable-state current (quasi-static approximation), there is a duality rule between the current field problem and the static electric field problem. This rule means that the current field ($\vec{J}^V$), which is accessible by the body surface recordings, can be characterized by a scalar quantity—potential (Φ) governed by Poisson's equation (Plonsey 1969, Gulrajani 1998)

$$\nabla^2 \Phi = \frac{\nabla \cdot \vec{J}^p}{\delta} = -\frac{I_V}{\delta} \tag{1}$$

where I_V is called the current source density (CSD). $\vec{J}$ ($\vec{J}^p$ and $\vec{J}^V$) is the current density (CD) in the strictly physical sense. Equation (1) shows that the current field ($\vec{J}^V$) or the potential (Φ) in the volume conductor is totally determined by the primary current density $\vec{J}^p$ (PCD) or CSD I_V. Here for illustration, considering PCD or CSD in a homogeneous volume conductor, we have (Plonsey 1969)

$$\Phi(\vec{r}) = \frac{1}{4\pi\delta} \int \vec{J}^p(\vec{r}') \cdot \frac{\vec{r} - \vec{r}'}{|\vec{r} - \vec{r}'|^3} \, \mathrm{d}\vec{r}'. \tag{2}$$

Equation (2) shows that a segment of the primary current density $\vec{J}^p \, \mathrm{d}\vec{r}'$ behaves like a dipole because it generates a field that varies as $1/r^2$, and a whole $\vec{J}^p$ behaves like a dipole distribution.

Apparently, this fact provides strong physiological evidence for the dipole model used in the biological electromagnetic field problem.

Meanwhile, according to equation (1), we have

$$\Phi(\vec{r}) = \frac{1}{4\pi\delta}\int \frac{\nabla\cdot\vec{J}^{p}(\vec{r}')}{|\vec{r}-\vec{r}'|}\,\mathrm{d}\vec{r}' = \frac{1}{4\pi\delta}\int \frac{-I_v}{|\vec{r}-\vec{r}'|}\,\mathrm{d}\vec{r}'. \tag{3}$$

Here CSD behaves like a charge because it generates a field that varies as $1/r$, so it provides physiological evidence of the effective charge model. It is the end point of the primary current, which flows in a neuron, i.e. the cell membrane where the current source density I_V appears.

In summary, the actual sources representing the neural electric activities are the PCD or the CSD, and the actual accessible physical quantity is the current field which arrives at the scalp surface. However, due to the duality rule between the current field problem and the static electric field problem (Plonsey 1969), their counterparts—the dipole, charge and potential—are widely accepted in current practice of biological electric forward and inverse problems.

In this paper, our main focus is the equivalent representation of the neural electric activities in the brain by a charge layer whose spatial distribution is of higher resolution than that of the scalp potential. The contents include the forward theory of ECL and EDL for neural electric sources in a 4-concentric-sphere head model, and the comparison between ECL and EDL in theory, simulation and real evoked data tests.

2. Forward theory

2.1. Forward theory of a charge or a dipole in an infinite medium

The potential distribution of an arbitrarily positioned and orientated dipole in an infinite medium is given by the following set of formulae (Yao 2001):

$$\Phi_\infty = \frac{1}{4\pi\delta_1}\vec{P}\cdot\nabla_{r_0}\left(\frac{1}{r_p}\right) = \sum_{l,m}\frac{1}{r^{l+1}}S_l^m(\vec{P},\theta,\varphi) \qquad r > r_0 \tag{4}$$

$$\begin{aligned}\frac{1}{r_p} = \frac{1}{\sqrt{r^2+r_0^2-2rr_0\cos\theta_0}} &= \sum_{l=0}^{\infty}\frac{r_0^l}{r^{l+1}}P_l(\cos\theta_0) = \sum_{l=0}^{\infty}\frac{r_0^l}{r^{l+1}}\sum_{m=0}^{l}(2-\delta_{m0})\frac{(l-m)!}{(l+m)!}\\ &\quad\times(\cos m\varphi\cos m\varphi_0+\sin m\varphi\sin m\varphi_0)P_l^m(\cos\theta)P_l^m(\cos\theta_0)\\ &= \sum_{l=0}^{\infty}\frac{r_0^l}{r^{l+1}}\sum_{m=0}^{l}(2-\delta_{m0})(\cos m\varphi\cos m\varphi_0+\sin m\varphi\sin m\varphi_0)\\ &\quad\times\tilde{P}_l^m(\cos\theta)\tilde{P}_l^m(\cos\theta_0)\end{aligned}$$

where

$$S_l^m(\vec{P},\theta,\varphi) = \left(g_l^m(\vec{P},\vec{r}_0)\cos m\varphi + h_l^m(\vec{P},\vec{r}_0)\sin m\varphi\right)\tilde{P}_l^m(\cos\theta) \tag{5}$$

$$\begin{aligned}g_l^m(\vec{P},\vec{r}_0)+\mathrm{j}h_l^m(\vec{P},\vec{r}_0) = \frac{r_0^{l-1}}{4\pi\delta_1}(2-\delta_{m0})\Bigg(&lP_r\tilde{P}_l^m(\cos\theta_0)+\frac{mP_\varphi}{\sin\theta_0}\tilde{P}_l^m(\cos\theta_0)\,\mathrm{e}^{\mathrm{j}\pi/2}\\ &-\frac{P_\theta}{2}\left(\sqrt{(l-m+1)(l+m)}\,\tilde{P}_l^{m-1}(\cos\theta_0)\right.\\ &\left.-\sqrt{(l-m)(l+m+1)}\,\tilde{P}_l^{m+1}(\cos\theta_0)\right)\Bigg)\mathrm{e}^{\mathrm{j}m\varphi_0} \qquad \mathrm{j}=\sqrt{-1}\end{aligned} \tag{6}$$

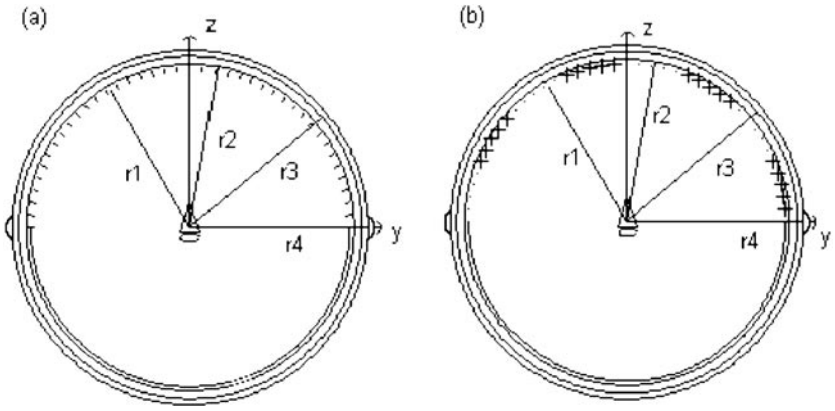

Figure 1. Concentric 4-sphere conductor head model and equivalent source layer. In this model, the radii are $r_1 = 7.9$ cm, $r_2 = 8.1$ cm, $r_3 = 8.5$ cm and $r_4 = 8.8$ cm for the outer boundaries of the inner brain sphere (grey), the cerebrospinal fluid layer (white), the skull layer (black) and the scalp layer (grey), respectively. And the conductivities are 0.461 A (V m)$^{-1}$, 1.39 A (V m)$^{-1}$, 0.0058 A (V m)$^{-1}$ and 0.461 A (V m)$^{-1}$, respectively. (a) The discrete equivalent dipole layer on the upper hemisphere with $r_T = r_1$ where the dipoles (bars) are oriented normal to the surface, (b) the discrete equivalent charge layer on the upper hemisphere with $r_T = r_1$ where the sum of positive (+) and negative (−) charges is zero. The mid-point between the left and right preauricular points is defined as the Cartesian coordinate origin. The axis directed away from the origin towards the left preauricular point is defined as the $+y$ axis, and that from the origin to the nasion the $+x$ axis. The $+z$ axis is defined as the axis that is perpendicular to both these axes and directed from the origin to the vertex.

and

$$\tilde{P}_l^m = \sqrt{\frac{(l-m)!}{(l+m)!}} P_l^m \tag{7}$$

where $(r_0, \theta_0, \varphi_0)$ is the location of a dipole within the inner brain, (r, θ, φ) are the spherical coordinates of the location of a field point and r_p is the distance between the dipole source location and the field point. P_l^m is the associated Legendre function of degree l and order m, and $\tilde{P}_l^m$ is the normalized associated Legendre function. $\delta_1$is the conductivity of the inner brain in figure 1. δ_{m0} is the Kronecker delta, $\delta_{m0} = 0\,(m \neq 0)$, $\delta_{00} = 1$. $\vec{P}(P_r, P_\theta, P_\varphi)$ is the dipole moment in the spherical coordinate system. Practically, the degree l is terminated at an integer value, which is 150 in this work.

Similarly, for a charge I located at $(r_0, \theta_0, \varphi_0)$, the potential will be (He *et al* 2002b)

$$\Phi_\infty = \frac{I}{4\pi\delta_1}\frac{1}{r_p} = \sum_{l,m} \frac{1}{r^{l+1}} S_l^m(I, \theta, \varphi) \qquad r > r_0 \tag{8}$$

where

$$S_l^m(I, \theta, \varphi) = \left(g_l^m(I, \vec{r}_0)\cos m\varphi + h_l^m(I, \vec{r}_0)\sin m\varphi\right)\tilde{P}_l^m(\cos\theta) \tag{9}$$

and

$$g_l^m(I, \vec{r}_0) + \mathrm{j}h_l^m(I, \vec{r}_0) = \frac{r_0^l}{4\pi\delta_1}(2 - \delta_{m0}) I \tilde{P}_l^m(\cos\theta_0)\,\mathrm{e}^{\mathrm{j}m\varphi_0} \qquad \mathrm{j} = \sqrt{-1}. \tag{10}$$

Comparing equations (4)–(5) and (9)–(10), we find that the representations are similar to each other.

2.2. Forward theory of a charge or a dipole in a concentric 4-sphere model

The head is modelled as a concentric 4-sphere model (figure 1). The conductivities and radii shown were taken from Cuffin and Cohen (1977). In this model, the radii are 7.9 cm, 8.1 cm, 8.5 cm and 8.8 cm, respectively, for the outer boundaries of the inner brain sphere, the cerebrospinal fluid layer (CSF), the skull layer and the scalp layer. And the conductivities are 0.461 A (V m)$^{-1}$, 1.39 A (V m)$^{-1}$, 0.0058 A (V m)$^{-1}$ and 0.461 A (V m)$^{-1}$, respectively.

Due to the similarity between (4) and (10), the general formula shown below may be used to derive the representation of the potential in a concentric 4-sphere model:

$$\Phi_\infty = \sum_{l,m} \frac{1}{r^{l+1}} S_l^m \qquad r > r_0. \tag{11}$$

Based on the electrostatic boundary condition of the concentric 4-sphere volume conductor that the potential and normal current are continuous across the boundaries (Yao 2001), the expression of the potential in each spherical shell is

$$\begin{aligned}\Phi(i) &= \sum_{l,m} \frac{W_l(i)}{r^{l+1}} S_l^m \\ &= \sum_{l,m} \frac{1}{r^{l+1}} \left(U_l^m(i)\cos m\varphi + V_l^m(i)\sin m\varphi\right) \tilde{P}_l^m(\cos\theta)\end{aligned} \tag{12}$$

$$U_l^m(i) = W_l(i) g_l^m \qquad V_l^m(i) = W_l(i) h_l^m \tag{13}$$

$$7.9 \geqslant r > r_0 \quad i = 1 \qquad 8.1 \geqslant r \geqslant 7.9 \quad i = 2$$
$$8.5 \geqslant r \geqslant 8.1 \quad i = 3 \qquad 8.8 \geqslant r \geqslant 8.5 \quad i = 4$$

where $i = 1, 2, 3, 4$ represent the inner brain, the cerebrospinal fluid layer, skull layer and scalp layer, respectively (figure 1). For the scalp surface, we have

$$W_l(4) = G_l {r_4}^{2l+1}(1+k) \tag{14}$$

$$G_l = \frac{1}{r_1^{2l+1}} \frac{1+s}{1+kr_{43}^{2l+1}} \frac{1+\gamma}{1+sr_{32}^{2l+1}} \frac{2l+1}{l(1-f_1)+\gamma r_{21}^{2l+1}[l+f_1(l+1)]} \tag{15}$$

$$p = r_{34}^{2l+1}(1-f_3) - (1+kf_3) \qquad q = (1-f_3) - r_{34}^{2l+1}(1+k^{-1}f_3) \tag{16}$$

$$\alpha = k\, r_{23}^{2l+1}(f_2 - 1) + s(kf_2 + 1) \tag{17}$$

$$\beta = r_{23}^{2l+1}(k + f_2) + s(1 + f_2) \tag{18}$$

and

$$\begin{aligned}&\gamma = \alpha/\beta \qquad f_1 = \sigma_2/\sigma_1 \qquad s = p/q \qquad k = l(l+1)^{-1} \\ &f_2 = \sigma_2/\sigma_3 \qquad r_{34} = r_3/r_4 \qquad r_{43} = r_4/r_3 \qquad r_{32} = r_3/r_2 \\ &r_{23} = r_2/r_3 \qquad r_{21} = r_2/r_1 \qquad f_3 = \sigma_3/\sigma_4.\end{aligned} \tag{19}$$

Equations (14)–(19) show that the coefficient $W_l(4)$ is determined by the ratios of radii, and if normalized radii are used, the result will be similar except for a constant factor: for a dipole source, in equations (4) and (6), we have $\frac{r_0^{l-1}}{r^{l+1}} = \left(\frac{r_0}{r}\right)^{l-1} \frac{1}{r^2}$, where a constant factor $\frac{1}{r^2}$ remains that cannot be normalized; for a charge source, in equations (4) and (10), we have $\frac{r_0^l}{r^{l+1}} = \left(\frac{r_0}{r}\right)^l \frac{1}{r}$, where a constant factor $\frac{1}{r}$ remains that cannot be normalized.

2.3. Forward theory of spherical equivalent charge layer and dipole layer

2.3.1. General concept. The general equivalent layer source technique may be represented by the following integral (Yao and Luo 1996, Yao *et al* 2001):

$$\Phi(\vec{r};\vec{r}_0) = \oiint_{S_T} u_T(\vec{r}_T;\vec{r}_0)\Phi_u(\vec{r};\vec{r}_T)\,\mathrm{d}s_T = \Phi(\vec{r};\text{layer}). \tag{20}$$

Equation (20) shows that the potential $\Phi(\vec{r};\vec{r}_0)$ at $\vec{r}(r,\theta,\varphi)$ generated by a unit source at $\vec{r}_0(r_0,\theta_0,\varphi_0)$ is equal to the potential $\Phi(\vec{r};\text{layer})$ of a charge or a dipole layer on a spherical surface S_T with radius $r_T < r_1$ (inside the inner surface of CSF). $\Phi_u(\vec{r};\vec{r}_T)$ is the potential at $\vec{r}(r,\theta,\varphi)$ produced by a unit charge or a unit radial dipole located at $\vec{r}_T(r_T,\theta_T,\varphi_T)$ on S_T in the head model with moment $\vec{P}(P_r,\,P_\theta,\,P_\varphi) = \vec{P}(1.0,0.0,0.0)$. $u_T(\vec{r}_T;\vec{r}_0)$, determined by the actual unit charge or dipole at $\vec{r}_0(r_0,\theta_0,\varphi_0)$, is the density function at $\vec{r}_T(r_T,\theta_T,\varphi_T)$ of the unknown equivalent layer source, and it may be put in the following form in a spherical coordinate system:

$$u_T(\vec{r}_T;\vec{r}_0) = \sum_{l,m}\left(a_l^m\cos m\varphi_T + b_l^m\sin m\varphi_T\right)\tilde{P}_l^m(\cos\theta_T). \tag{21}$$

The forward theory we are going to establish is the detail of $u_T(\vec{r}_T;\vec{r}_0)$ so that we may calculate the equivalent source density when we know the actual sources.

2.3.2. Equivalent charge layer. For a unit charge, invoking equations (9) and (10) in (12), we get

$$\begin{aligned}\Phi_u(\vec{r};\vec{r}_T) = {}&\sum_{l,m}\frac{1}{r^{l+1}}\frac{r_T^l}{4\pi\delta_1}(2-\delta_{m0})W_l(i)\\ &\times\tilde{P}_l^m(\cos\theta_T)(\cos m\varphi_T\cos m\varphi+\sin m\varphi_T\sin m\varphi)\tilde{P}_l^m(\cos\theta).\end{aligned} \tag{22}$$

Invoking equations (21) and (22) in (20), we have

$$\begin{aligned}\Phi(\vec{r};\text{charge-layer}) = {}&\sum_{l,m}\sum_{l',m'}\frac{1}{r^{l+1}}\frac{r_T^l}{4\pi\delta_1}(2-\delta_{m0})W_l(i)\tilde{P}_l^m(\cos\theta)\\ &\times\int_0^{2\pi}\int_0^{\pi}\tilde{P}_l^m(\cos\theta_T)(\cos m\varphi_T\cos m\varphi+\sin m\varphi_T\sin m\varphi)\\ &\times\left(a_{l'}^{m'}\cos m'\varphi_T + b_{l'}^{m'}\sin m'\varphi_T\right)\tilde{P}_{l'}^{m'}(\cos\theta_T)r_T^2\sin\theta_T\,\mathrm{d}\theta_T\,\mathrm{d}\varphi_T.\end{aligned}$$

Using the orthogonal properties of the triangle function and the associated Legendre function, we get

$$\Phi(\vec{r};\text{charge-layer}) = \sum_{l,m}\frac{W_l(i)}{r^{l+1}}\frac{r_T^{l+2}}{\delta_1}\frac{1}{2l+1}\left(a_l^m\cos m\varphi + b_l^m\sin m\varphi\right)\tilde{P}_l^m(\cos\theta). \tag{23}$$

Comparing equation (12) with (23), we see that if

$$a_l^m = g_l^m\Big/\left(\frac{r_T^{l+2}}{\delta_1}\frac{1}{2l+1}\right)\qquad b_l^m = h_l^m\Big/\left(\frac{r_T^{l+2}}{\delta_1}\frac{1}{2l+1}\right) \tag{24}$$

equation (23) will be the same as equation (12). This fact means that the spherical equivalent charge-layer source produces the same potential as the actual source does. Thus after invoking equation (24) in equation (21), we get the forward theory of the equivalent charge-layer source:

$$u_T(\vec{r}_T;\vec{r}_0) = \sum_{l,m}\frac{\delta_1}{r_T^{l+2}}(2l+1)\left(g_l^m\cos m\varphi_T + h_l^m\sin m\varphi_T\right)\tilde{P}_l^m(\cos\theta_T). \tag{25}$$

2.3.3. Equivalent dipole layer. Invoking $\vec{P}(P_r, P_\theta, P_\varphi) = \vec{P}(1.0, 0.0, 0.0)$ in equation (6), and then invoking equations (5) and (6) in equation (12), we get

$$\Phi_u(\vec{r}; \vec{r}_T) = \sum_{l,m} \frac{1}{r^{l+1}} \frac{r_T^{l-1}}{4\pi\delta_1}(2 - \delta_{m0}) l W_l(i) \tilde{P}_l^m(\cos\theta_T) \times (\cos m\varphi_T \cos m\varphi + \sin m\varphi_T \sin m\varphi) \tilde{P}_l^m(\cos\theta). \tag{26}$$

Invoking equations (21) and (26) in equation (20), we have

$$\begin{aligned}\Phi(\vec{r}; \text{dipole-layer}) = {} & \sum_{l,m} \sum_{l',m'} \frac{1}{r^{l+1}} \frac{r_T^{l-1}}{4\pi\delta_1}(2 - \delta_{m0}) l W_l(i) \tilde{P}_l^m(\cos\theta) \\ & \times \int_0^{2\pi} \int_0^{\pi} \tilde{P}_l^m(\cos\theta_T)(\cos m\varphi_T \cos m\varphi + \sin m\varphi_T \sin m\varphi) \\ & \times \left(a_{l'}^{m'} \cos m'\varphi_T + b_{l'}^{m'} \sin m'\varphi_T\right) \tilde{P}_{l'}^{m'}(\cos\theta_T) r_T^2 \sin\theta_T \, \mathrm{d}\theta_T \, \mathrm{d}\varphi_T.\end{aligned}$$

Using the orthogonal properties of the triangle function and the associated Legendre function, we get

$$\Phi(\vec{r}; \text{dipole-layer}) = \sum_{l,m} \frac{1}{r^{l+1}} \frac{r_T^{l+1}}{\delta_1} W_l(i) \frac{l}{2l+1} \left(a_l^m \cos m\varphi + b_l^m \sin m\varphi\right) \tilde{P}_l^m(\cos\theta). \tag{27}$$

Comparing equations (27) with (12), we see that if

$$a_l^m = g_l^m \Big/ \left(\frac{r_T^{l+1}}{\delta_1} \frac{l}{2l+1}\right) \qquad b_l^m = h_l^m \Big/ \left(\frac{r_T^{l+1}}{\delta_1} \frac{l}{2l+1}\right) \tag{28}$$

equation (27) will be the same as equation (12). This fact means that the spherical equivalent dipole-layer source produces the same potential as the actual source does. Thus, after invoking equation (28) in equation (21), we get the forward theory of the equivalent dipole-layer source:

$$u_T(\vec{r}_T; \vec{r}_0) = \sum_{l,m} \frac{\delta_1}{r_T^{l+1}} \frac{2l+1}{l} \left(g_l^m \cos m\varphi_T + h_l^m \sin m\varphi_T\right) \tilde{P}_l^m(\cos\theta_T). \tag{29}$$

2.3.4. Summary. For the circumstance when there are Q real sources with strength s_q, $q = 1, \ldots, Q$, the overall potential at $\vec{r}(r, \theta, \varphi)$ is

$$\Phi(\vec{r}) = \sum_{q=1}^{Q} s_q \Phi(\vec{r}; \vec{r}_0(q)) \tag{30}$$

and the theoretical integral equation (20) of equivalent layer changes to

$$\Phi(\vec{r}) = \oiint_{S_T} U_T(\vec{r}_T) \Phi_u(\vec{r}; \vec{r}_T) \, \mathrm{d}s_T = \Phi(\vec{r}; \text{layer}) \tag{31}$$

where the total equivalent source strength is

$$U_T(\vec{r}_T) = \sum_{q=1}^{Q} s_q u_T(\vec{r}_T; \vec{r}_0(q)). \tag{32}$$

Equation (31) shows that the potential of the real sources is equal to that of a continuous layer source. And the forward calculation of the equivalent layer density can be implemented by equations (25) and (32) for a charge layer, or equations (29) and (32) for a dipole layer.

The related forward calculation of the potential produced by charge source and dipole source can be implemented by equations (10) and (6), respectively.

In early published work, due to the lack of a forward theory of the equivalent layer source, the feasibility of ECL and EDL was mainly evaluated by comparing the actual cortical surface potential with the reconstructed cortical surface potential (Sidman *et al* 1992, Yao 1996). And based on a local equivalent concept, Amir (1994) suggested that the discrete distributed dipoles should not be oriented along the normal direction of the equivalent source surface in general. The forward theory, originally developed in 1996 (Yao and Luo 1996) for a single sphere model and newly extended to the 4/3-concentric-sphere head model shown here and in Yao *et al* (2001), provides the theoretical base of ECL and EDL, because the forward formulae of the layer source density demonstrate the correctness of the equivalence assumption between the real sources and the equivalent layer with charge or dipole oriented normal to the layer surface. Based on this theory, the theoretical value of the equivalent layer source that produces the same potential as the actual sources can be calculated analytically according to equations (25) and (29). And so the ECL and EDL estimate can be evaluated not only by the empirical comparison between the cortical-surface potential produced by the equivalent layer source and that by the actual sources (Sidman *et al* 1992, Yao 1996), but also by the direct comparison between the inverse equivalent layer source and the forward equivalent layer source. Such a direct comparison can be used to select a good one among all algorithms that can be used to conduct the inversion (Yao *et al* 2001).

3. Simulation tests

3.1. Forward calculation

In the simulation calculations, the mid-point between the left and right preauricular points is defined as the Cartesian coordinate origin. The axis directed away from the origin towards the left preauricular point is defined as the $+y$ axis, and that from the origin to the nasion the $+x$ axis. The $+z$ axis is defined as the axis that is perpendicular to both these axes and directed from the origin to the vertex.

The forward calculations are based on equations (12)–(14) and equation (6) for the scalp potential produced by dipole sources, equations (12)–(14) and equation (10) for the scalp potential produced by charge sources, equation (25) for ECL and equation (29) for EDL.

3.2. Inverse of layer source

Equation (20) can be written in a discrete form

$$\Phi(\vec{r}_j) = \sum_{n=0}^{N} S_n \Phi_u(\vec{r}_j; \vec{r}_T(n)) \qquad j = 1, \ldots, M \tag{33}$$

where N is the number of discrete equivalent sources, in this work it is 3000, and they are assumed to be uniformly distributed on the upper hemisphere surface of the sphere with radius $r_T = 7.9$ cm. S_n is the strength of the discrete equivalent source. $\Phi_u(\vec{r}_j, \vec{r}_T(n))$ is represented by equations (22) and (26), which is the transfer function from a unit charge or a unit radial dipole source located at $\vec{r}_T(n)(r_T(n), \theta_T(n), \varphi_T(n))$ to a measurement electrode position $\vec{r}_j(r_j, \theta_j, \varphi_j)$ (Sidman *et al* 1992, Yao 1996). M is the number of the electrodes, which is 120 in our simulation, and their positions are obtained from actual EEG recording electrode positions projected onto a sphere surface with radius 8.8 cm. Based on the recordings

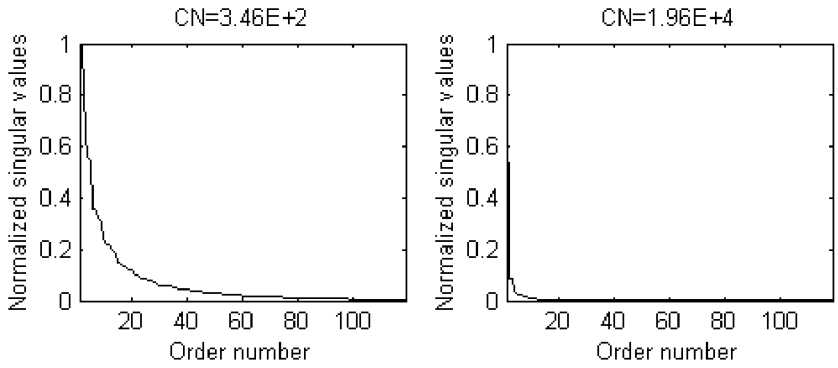

Figure 2. Normalized singular value distributions of EDL inversion and ECL inversion. Left: EDL; right: ECL. The horizontal axis is the order number of the singular values. CN is defined as the ratio of the first singular value to the last singular value.

$\Phi(\vec{e}_j)$ derived from the scalp electrodes $\vec{r}_j = \vec{e}_j(r_j = 8.8 \text{ cm}, \theta_j, \varphi_j),\ j = 1, \ldots, M$, we have

$$\Phi(\vec{e}_j) = \sum_{n=0}^{N} S_n \Phi_u(\vec{e}_j; \vec{r}_T(n)) \qquad S_n = U_T(\vec{r}_T(n))\,\mathrm{d}s_T \qquad j = 1, \ldots, M \tag{34}$$

where both $\Phi(\vec{e}_j)$ and $\Phi_u(\vec{e}_j; \vec{r}_T(n))$ are known, the strength $S_n$of the discrete layer source may be found by a linear inversion of equation (34). In this work, the singular value decomposition (SVD) algorithm is used and the singular value truncation technique is used as the regularization tool for noisy scalp data. Besides, in order to mimic the actual EEG recording, we adopt an average reference, so the independent recordings $M - 1$, for $M = 120$, is 119.

Shown in figure 2 are the two normalized distributions of the singular values of the two techniques used in solving equation (34). The left figure illustrates the EDL inverse and the right one shows the ECL inverse. In the figures, the condition number (CN) is defined as the ratio of the first singular value to the last singular value. The CN value of the ECL inverse is about 100 times that of EDL, which foretells that the inverse calculation of ECL will be more sensible to noise than that of EDL.

Figure 3 shows the spatial spectra filters of the scalp potential, ECL and EDL. They are $W_l(4)$, shown by equation (14) for the scalp potential, $(2l + 1)$ shown by equation (25) for ECL, and $\frac{2l+1}{l}$ shown by equation (29) for EDL. They show that ECL has a filter with high spatial frequency amplification, while EDL and scalp potential are results of low-pass spatial filters.

It has been observed, on one hand, that the inverse calculation of ECL is more difficult than that of EDL (figure 2), and, on the other hand, ECL is of higher spatial resolution in theory than EDL (figure 3). These opposite characteristics of EDL and ECL mean that the practical performances of ECL and EDL will depend on the concrete algorithm adopted for the inverse calculation and on the noise level of the scalp recordings. In the following tests, the popular truncated SVD pseudo-inverse was used for both ECL and EDL inverses from both noiseless and noisy scalp data, and the results show that ECL has a little higher spatial resolution than that of EDL.

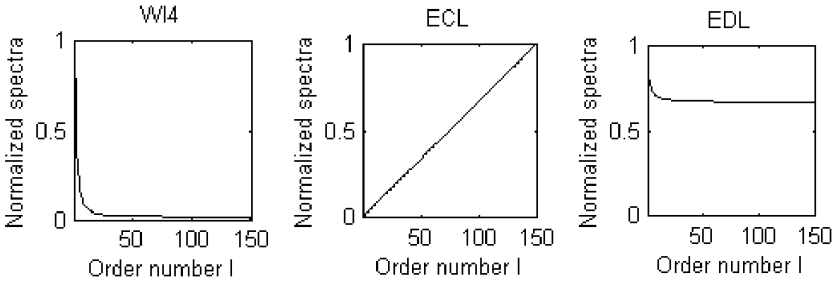

Figure 3. The normalized spatial spectra amplitude versus degree l of spatial filter $W_l(4)$ and the filters $(2l+1)$ and $(2l+1)/l$ of ECL and EDL shown in equations (22) and (26). The left figure is $W_l(4)$, the middle figure is ECL and the right figure is EDL.

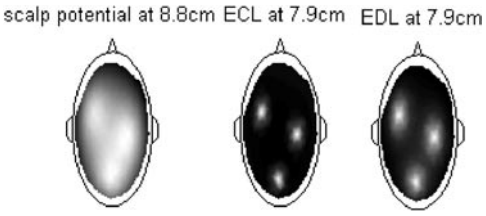

Figure 4. Forward maps of scalp potential and ECL, EDL of three assumed dipoles. Left: scalp potential at the scalp surface with radius 8.8 cm; middle: ECL at the cortical surface with radius 7.9 cm; right: EDL at the cortical surface.

3.3. Dipole sources test

Suppose that there are three unit radial dipoles ($Q = 3$) in the volume conductor model, the locations of which in Cartesian coordinates are respectively (x, y, z) = (–6.511 4726e–001, 3.955 7931e–002, 7.579 1979e–001) × 6.4 cm, (–6.493 0717e–002, –4.341 3298e–001, 8.985 0574e–001) × 6.4 cm and (2.183 6882e–001, 4.657 8965e–001, 8.575 2846e–001) × 6.4 cm. The forward scalp EEG map is shown in figure 4 (left). Apparently, due to the low-pass filter of the skull (Nunez *et al* 1994, Yao 2000), it is not easy to discriminate the three active regions. Shown in figure 4 (middle and right) are the forward ECL and EDL; both of them show much higher spatial resolution than the scalp potential map does, and ECL has the highest spatial resolution.

Figure 5 shows the inverse results, where (a) and (b) are for the noiseless case in which all 119 singular values are used in the inverse calculation, (c) and (d) are for the noisy case where Gaussian noise with noise–signal ratio 15% is added to the scalp recordings before the inverse. The inverse is conducted by truncated SVD pseudo-inverse, and the truncation is chosen at 23 where the ratio of the 23rd singular value to the first singular value is 0.1 for EDL inverse and 0.002 for ECL inverse. Figure 5 shows that ECL and EDL are reliably inverted as high-resolution imaging maps. For the noiseless case (figures 5(a) and (b)), it is clear that the reconstruction is very good and the ECL map has a little higher spatial resolution than the EDL map does. For the noisy case (figures 5(c) and (f)), though both ECL and EDL imaging maps are blurred because of the SVD truncation, the ECL map still is of a little higher spatial resolution than the EDL map, as shown by the relative better separability of the three sources.

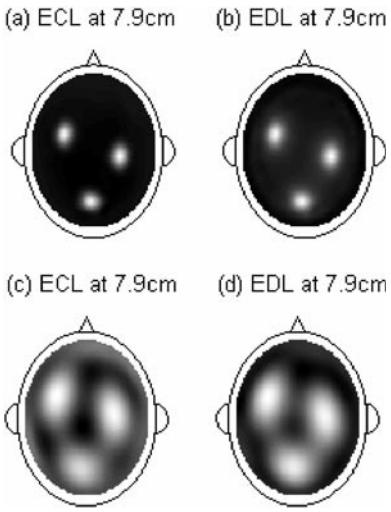

Figure 5. Reconstructed ECL and EDL maps of three assumed dipoles. (a) and (b) are reconstructed from scalp potential without noise; (c) and (d) are reconstructed from noisy scalp potential with 15% Gaussian noise added to the scalp potential.

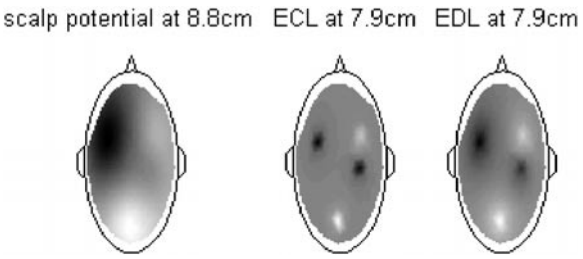

Figure 6. Forward maps of scalp potential and ECL, EDL of four assumed charges. Left: scalp potential at the scalp surface with radius 8.8 cm; middle: ECL at the cortical surface with radius 7.9 cm; right: EDL at the cortical surface.

3.4. Charge sources test

Suppose that there are four unit charges ($Q = 4$) in the volume conductor model; the locations in Cartesian coordinates are respectively (x, y, z) = (–6.511 4726e–001, 3.955 7931e–002, 7.579 1979e–001) × 7.1 cm, (–6.493 0717e–002, –4.341 3298e–001, 8.985 0574e–001) × 7.1 cm and (2.183 6882e–001, 4.657 8965e–001, 8.575 2846e–001) × 7.1 cm, (2.183 6882e–001, –4.657 8965e–001, 8.575 2846e−001) × 7.1 cm. The first and fourth ones are with positive unit charge, the second and third with negative unit charge, so the total charge is zero, which keeps overall neutrality of the source for the brain. Figure 6 (left) shows the forward scalp EEG map. Due to the low-pass filter of the skull shown by figure 3 (left), it is very difficult to discriminate the four active regions. The forward ECL and EDL maps are shown in figure 6 (middle and right). They reveal the four active sources clearly, especially the ECL.

Figure 7 shows the inverse results, where (a) and (b) are for the noiseless case, which are reconstructed without singular value truncation, (c) and (d) are for the noisy case where the same Gaussian noise ratio and the same truncated SVD pseudo-inverse are used as the dipole sources case discussed above. Figure 7 shows that both ECL and EDL can be used to

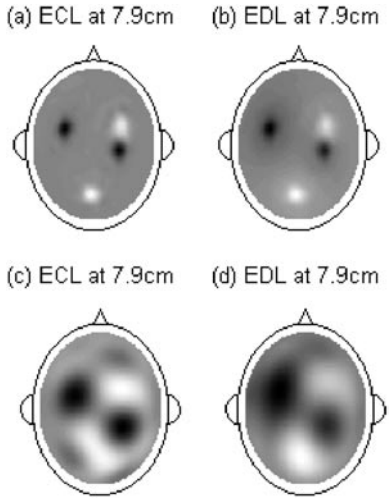

Figure 7. Reconstructed ECL and EDL maps of four assumed charges. (a) and (b) are reconstructed from scalp potential without noise and (c) and (d) are reconstructed from noisy scalp potential with 15% Gaussian noise added to the scalp potential.

Table 1. Correlation coefficients (CC) between the forward values and inverse values.

	Three dipoles		Four charges	
CC	ECL	EDL	ECL	EDL
Noiseless	0.9926	0.9812	0.9692	0.9815
15% noise	0.6213	0.9002	0.5991	0.9216

ECL: equivalent charge layer, EDL: equivalent dipole layer.

image charge sources. For the noiseless case, it is clear that each of the four sources is more locally imaged in ECL than in EDL. While for the noisy case, we see that the images of all four sources are smoothed, and the merit of ECL is that the relative amplitude relations among the four sources are kept better than those in the EDL map where the source (white in the map) near the right ear is almost lost.

Table 1 lists the correlation coefficients (CC) between the forward and inverse ECL and EDL values. It shows that EDL is easier to invert than ECL because of the difference of the singularity of the two inverses, as shown in figure 2. However, for high-resolution mapping, what we care about is the spatial resolution. The results shown above tell us that ECL is a meaningful imaging quantity to use, and much more effort should be paid to the inverse algorithm of ECL in the future.

4. Real EEG data test

119-channel ERP data are obtained. The stimulation in the right visual field is the picture shown in figure 8(a). Both the ERP data and electrode coordinate data are group averages of ten subjects. The averaged electrode coordinate values are further normalized to the unit sphere surface. The noise/signal ratio is estimated by using the recorded data before stimulation as the noise background, and the result is 14%. Figure 8(b) is the scalp ERP at 100 ms after the stimulation. Figures 8(c) and (d) are the reconstructed ECL and EDL maps. In the calculation,

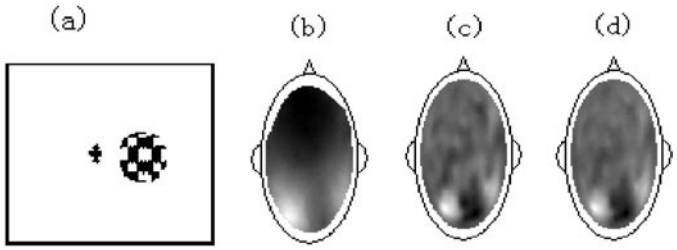

Figure 8. High-resolution EEG imaging maps from real EEG data. (a) The stimulus picture, (b) the real scalp potential at 8.8 cm, (c) the reconstructed ECL map at 7.9 cm and (d) the reconstructed EDL map at 7.9 cm.

truncated SVD pseudo-inverse with truncation at 22 is used. Comparing ECL and EDL with the scalp EEG, both ECL and EDL offer a higher spatial resolution map, and both of them are consistent with the visual gateway theory when the stimulation appears in the right visual field; the main reaction is located on the left visual cortex. In this example, ECL and EDL are similar to each other by a correlation coefficient 0.9560.

5. Conclusion and discussion

Equivalent layer source imaging is one of the recently suggested new imaging modalities. They are presented not only because of their practical efficiencies as shown above but also because of their clear physical meaning. In fact, the forward theory of ECL and EDL shown above clearly affirms them being unique representations of the actual sources underneath the layer and being independent of the complexity of the outer medium of the actual head model, i.e. the filters shown in figure 3 (middle and right) are independent of the head model. Apparently, in this sense, ECL, EDL and SPM (Yao 2001) are similar and prior to CPM and LM which are decided not only by the actual sources but also by the head model. Besides, if we approximately assume that the sources of our interest are on the cortical surface, the EDL and ECL may be considered as an approximate inversion of the actual sources.

The above numeric and real data tests confirm that ECL and EDL are of higher spatial resolution than the scalp potential map and so of practical significance. In addition, EDL has been realized in a real head model (Babiloni *et al* 1997). ECL can be extended to a real head shape, too, so ECL and EDL can be expediently reconstructed from simulated data on a real head model or practical recordings. When comparing EDL and ECL, due to the divergence relation between the $\vec{J}^p$(dipole) and I_V(charge) $= \nabla \cdot \vec{J}^p$, we see that ECL is of higher spatial resolution though, due to the bad nature of the ECL inverse, a more robust algorithm is desired so that the merit of ECL can be better realized in the future.

Finally, let us continue some more discussions on source modelling. If we temporarily leave the resolution problem out, the actual problem is when a charge model (strictly a 'current source density' model) or a dipole model (strictly a primary 'current density' model) should be chosen. In general, both the charge model and the dipole model are phenomenological descriptions of the actual neuron electrical activities, so the choice depends on your concern. First, the approximation of a model to the actual neural electric activities may be different on different spatial scales. For example, for an excited single neuron cell, both positive and negative (current source density) charges exist on its cell membrane (the surface of the cell body, axon and dendrites). When the spatial distance between a positive charge and a negative charge is large enough, a model with paired charges is a proper choice; otherwise, an integrated

dipole formed by the paired positive and negative charges is a proper model. Secondly, the dipole model or charge model used in EEG inverse is in the sense of macro scale average, and so the approximation also depends on the combination of neurons and shape of each neuron. For focal parallel small scale neuron combinations, a dipole model may be the best; for parallel large scale neuron combinations (with long dendrites and axon), a paired charges model may be a proper choice, and if the neurons are randomly distributed in a focal region, a quadrupole or even higher order model may be better than a paired charges model or a dipole model. Thirdly, the choice of source model also depends on the problem to be solved; for example, if the model is used as a macro description of the actual focal neural electric activities, such as the case of three-dimensional EEG imaging, the conducted research shows that the charge source model is better than the dipole source model in saving two thirds of the mass computation (Yao and He 1998, He *et al* 2002). If the model is used as an intermediate quantity to calculate other physical quantities such as the cortical surface potential or an imaging quantity, such as the case shown in this paper, the effectiveness depends on the uniqueness of the representation of the actual sources, and on the practical feasibility including calculation and interpretation. The results shown above confirm that ECL may be used as an efficient imaging modality, and previous works confirm its utility as an intermediate step to get the cortical surface potential (Yao 1996).

In summary, both current density (dipole) and current source density (charge) may be considered as the basic brain electric source model. If a charge model is chosen, it should be a positive and negative charge combination so that the total charge may be kept zero.

Acknowledgments

The author wishes to thank Drs B He, F Q Zhao, D S Wu, J Lian, F S Meng and X Hu for discussions on high-resolution EEG mapping, and also thanks Professor Chen and Mr Ao for help in collecting the real ERP data. He thanks the reviewers for fruitful comments. This work is supported by NSFC nos 90208003 and 30200059, TRAPOYT, Key Research Project of Science and Technology of MOE, China Sichuan Youth Researcher Foundation, Doctor Training Fund of MOE, PR China.

References

Amir A 1994 Uniqueness of the generators of brain evoked potential maps *IEEE Trans. Biomed. Eng.* **41** 1–11

Babiloni F, Babiloni C, Carducci F, Fattorini L, Anello C, Onorati P and Urbano A 1997 High resolution EEG: a new model-dependent spatial deblurring method using a realistically-shaped MR-constructed subject's head model *Electroenceph. Clin. Neurophysiol.* **102** 69–80

Babiloni F, Carducci F, Cincotti F, Del Gratta C, Roberti G M, Romani G L, Rossini P M and Babiloni C 2000 Integration of high resolution EEG and functional magnetic resonance in the study of human movement-related potentials *Methods Inf. Med.* **39** 179–82

Cuffin B N and Cohen D 1977 Magnetic fields of a dipole in spherical volume conductor shapes *IEEE Trans. Biomed. Eng.* **24** 372–81

Dale A M and Sereno M I 1993 Improved localization of cortical activity by combining EEG and MEG with MRI cortical surface reconstruction: a linear approach *J. Cogn. Neurosci.* **5** 162–76

Gulrajani R M 1998 *Bioelectricity and Biomagnetism* (New York: Wiley)

Hamalainen M and Ilmoniemi R 1984 Interpreting measured magnetic fields of the brain: estimates of current distributions *Tech Rep* TKF-F-A559 Helsinki University of Technology

He B, Yao D and Lian J 2002a High-resolution EEG: on the cortical equivalent dipole layer imaging *Clin. Neurophysiol.* **113** 227–35

He B, Yao D and Lian J 2002b An equivalent current source model and Laplacian weighted minimum norm current estimates of brain electrical activity *IEEE Trans. Biomed. Eng.* **49** 277–88

Hjorth B 1975 An online transformation of EEG scalp potentials into orthogonal source derivations *Electroenceph. Clin. Neurophysiol.* **39** 526–30

Niedermeyer E and Lopes da Silva F 1999 *Electroencephalography Basic Principles, Clinical Applications and Related Fields* 4th edn (Baltimore, MD: Williams and Wilkins)

Nunez P L 1987 Removal of reference electrode and volume conductor effects by spatial deconvolution of evoked potentials using a three concentric sphere model of the head *Electroenceph. Clin. Neurophysiol.* **39** (*Suppl.*) 143–8

Nunez P L 1989 Estimation of large scale neocortical source activity with EEG surface Laplacians *Brain. Topogr.* **2** 141–54

Nunez P L, Silberstein R B, Cadusch P J, Wijesinghe R S, Westdorp A F and Srinivasan R 1994 A theoretical and experimental study of high resolution EEG based on surface Laplacian and cortical imaging *Electroenceph. Clin. Neurophysiol.* **90** 40–57

Plonsey R 1969 *Bioelectric Phenomena* (New York: McGraw-Hill)

Sidman R D *et al* 1992 Experimental tests of the cortical imaging technique *IEEE Trans. Biomed. Eng.* **39** 437–44

Wang J Z, Williamson S J and Kaufman L 1992 Magnetic source images determined by a lead-field analysis: the unique minimum-norm least-squares estimation *IEEE Trans. Biomed. Eng.* **39** 665–75

Yao D 1996 The equivalent source technique and cortical imaging *Electroenceph. Clin. Neurophysiol.* **98** 478–83

Yao D 2000 High-resolution EEG mappings: a spherical harmonic spectra theory and simulation results *Clin. Neurophysiol.* **111** 81–92

Yao D 2001 Source potential mapping: a new modality to image the neural electrical activities *Phys. Med. Biol.* **46** 3177–89

Yao D 2002a High-resolution EEG mapping: a radial-basis function based approach to the scalp Laplacian estimate *Clin. Neurophysiol.* **113** 956–67

Yao D 2002b The theoretical relation of scalp Laplacian and scalp current density of a spherical shell head model *Phys. Med. Biol.* **47** 2179–85

Yao D and He B 1998 The Laplacian weighted minimum norm estimate of three dimensional equivalent charge distribution in the brain *Proc. Ann. Int. Conf. IEEE Engineering in Medicine and Biology Society* vol 20 pp 2108–11

Yao D and Luo B 1996 Theory of the EEG cortical imaging techniques *Chin. J. Biomed. Eng.* (Engl. Edn) **5** 128–36

Yao D, Zhou Y, Zeng M, Fan S, Lian J, Wu D, Ao X, Chen L and He B 2001 A study on equivalent source techniques of high-resolution EEG imaging *Phys. Med. Biol.* **46** 2255–66